NANOSYSTEMS:
PHYSICS, CHEMISTRY, MATHEMATICS

Original article

Kapishnikov A.V., Gerasimov E.Yu. *Nanosystems: Phys. Chem. Math.*, 2025, **16** (1), 51–57.
http://nanojournal.ifmo.ru
DOI 10.17586/2220-8054-2025-16-1-51-57

Phase transformations in perovskites $La_{0.6}Ca_{0.4}Mn_{1-y}Co_yO_{3\pm\delta}$ under the action of hydrogen

Alexander V. Kapishnikov, Evgeny Yu. Gerasimov

Boreskov Institute of Catalysis SB RAS, Novosibirsk, Russia

Corresponding author: E. Yu. Gerasimov, gerasimov@catalysis.ru

PACS 81.30.Bx

ABSTRACT The structural and phase transformations of $La_{0.6}Ca_{0.4}Mn_{1-y}Co_yO_{3\pm\delta}$ ($y = 0.2 - 0.6$) solid solutions in a reducing atmosphere were studied using in situ XRD and HRTEM methods. Experiments have shown that heat treatment in a reducing atmosphere of H_2 leads to the partial decomposition of solid solutions, the nature of which differs from decomposition in an inert atmosphere. In the case of a system with a hydrogen-containing atmosphere, the heterogeneous reduction of the structure leads to the formation of an orthorhombic phase of $LaMnO_3$-based perovskite with disordered vacancies, an additional phase of ordered Rudlesden–Popper-type perovskite based on La_2CoO_4 and Co and Ca_2MnO_4 nanoparticles on the surface of perovskite. In an environment with excessive partial oxygen pressure for the reduced sample, the reverse phase transition of the Rudlesden–Popper phase into the perovskite phase occurs.

KEYWORDS Rudlesden–Popper-type perovskite, hydrogen reduction, lanthanum manganite, in situ XRD, phase transition

ACKNOWLEDGEMENTS This study was supported by Russian Science Foundation, project No. 23-23-00535. XRD and HRTEM measurements were performed using the equipment of the Shared Research Center "National Center of Investigation of Catalysts" at the Boreskov Institute of Catalysis Siberian Branch, Russian Academy of Sciences.

FOR CITATION Kapishnikov A.V., Gerasimov E.Yu. Phase transformations in perovskites $La_{0.6}Ca_{0.4}Mn_{1-y}Co_yO_{3\pm\delta}$ under the action of hydrogen. *Nanosystems: Phys. Chem. Math.*, 2025, **16** (1), 51–57.

1. Introduction

Complex oxides with a perovskite structure have great potential for the synthesis and research of new compounds of this type, due to their structural flexibility [1–3]. They are widely used as catalysts for various reactions, in particular, reactions of high-temperature oxidation of hydrocarbons [4–6], decomposition of nitrogen oxides [7–9], in the processes of photocatalytic production of hydrogen [10–12] or the disposal of antibiotics in wastewater [13, 14]. In many ways, these properties are provided by structural features, in particular, the presence and distribution of cationic and anionic vacancies [15, 16]. The most common method of influencing the perovskite structure is to obtain solid solutions by replacing part of the cations with a lower charge state [17,18]. This leads to a decrease in the energy of vacancy formation, an increase in the level of nonstoichiometry [19, 20] and, as a result, to an increase in the activity of catalysts in oxidation reactions [21, 22].

Another way to create the required level of nonstoichiometry may be heat treatment of a complex oxide under reducing conditions. In the presence of cations of variable valence [23, 24], a decrease in the degrees of oxidation (as a rule, in the B-sublattice) will lead to irreversible removal of lattice oxygen and the formation of vacancies. The initial structure during these processes can either be preserved, undergoing minor changes in structural parameters [25], or be partially destroyed [26] with the formation of new phases. In this case, nanoparticles of new phases can form on the surface of perovskite-like oxides, which also affect their catalytic activity [27]. Thus, the catalytic activity of perovskites can increase simultaneously due to an increase in the level of nonstoichiometry in the structure and mobility of lattice oxygen, as well as due to the formation of a "carrier-active component" type system on the surface with partial decomposition of the initial phase. On the other hand, additional temperature exposure in a reducing atmosphere can lead to partial decomposition of solid solutions and can lead to negative consequences, in particular, to a decreasing of catalytic activity.

In this regard, studies of phase transformations of mixed oxides (for example, La–Ca–Mn–Co–O) are of interest for understanding their mechanisms and possibilities of controlling the reduction process to obtain more active systems or to search for optimal conditions for impact on initial solid solutions.

2. Experimental section

$La_{0.6}Ca_{0.4}Mn_{1-y}Co_yO_3$ sample was synthesized by the polymerizable precursor method. Appropriate amounts of crystal hydrates of salts, including $La(NO_3)_3 \cdot 6H_2O$ (ZRM, > 99 %), $Ca(NO_3)_2 \cdot 4H_2O$ (Merck, > 99 %), $Mn(NO_3)_2 \cdot 4H_2O$ (Merck, > 99 %), $Co(NO_3)_2 \cdot 6H_2O$ (Merck, > 99 %), citric acid (ChimProm, > 99.5 %), ethylene glycol (ChimProm, > 99.5 %), and distilled water were mixed. An aqueous solution with appropriate cation ratio La:Ca:Mn:Co was prepared. The resulting reagent was evaporated at 70 – 80 °C until the formation of a resinous polymer. The precursor was calcined at 800 °C for four hours with a rise in temperature of 100 °C/h.

The microstructure of the photocatalysts was studied by HRTEM using a ThemisZ electron microscope (Thermo Fisher Scientific, Waltham, MA, USA) at an accelerating voltage of 200 kV. The microscope was equipped with a SuperX energy-dispersive spectrometer and a spherical aberration corrector. The maximum resolution of the microscope was 0.06 nm. For the HRTEM analysis, the samples were ultrasonically dispersed onto perforated carbon substrates attached to copper grids.

XRD patterns were obtained on a Bruker AXS D8 Advance diffractometer (Karlsruhe, Germany) equipped with a high temperature, supply of various gas mixtures, the use of CuKα radiation in scanning with a step of $2\theta = 0.05^\circ$ point by point, and an ac-cumulation time of 3 s at each point in a range of the angles $2\theta = 15 - 75^\circ$. Temperature measurements were performed according to the following conditions: temperature rate of 10 °C/min with 30 % H_2 + 70 % He flow and a mixture rate of 40 mL/min. Dif-fractograms were obtained at temperatures of 30, 300, 450, 600 and 750 °C. The crystallite sizes and chemical compositions were calculated in the X'Pert HighScore Plus (PANalytical B.V., Almelo, The Netherlands) software. The calculation and refinement of lattice parameters were performed in the IK (BIC SB RAN, Novosibirsk, Russia) software by the method of least squares.

Thermal analysis of the sample was performed using a synchronous thermal analysis device, STA 449C Jupiter (NETZSCH, Selb, Germany). This device combines the methods of differential thermal analysis (DTA) and thermogravimetric analysis (TGA) into one dimension. The weight of the sample was approximately 100 mg. The furnace temperature was increased from 40 to 900 °C at a rate of 10 °C/min with He flux of 30 mL/min. The sample weight was monitored continuously as a function of temperature.

3. Results and discussions

The samples of the $La_{0.6}Ca_{0.4}Mn_{1-y}Co_yO_{3\pm\delta}$ series, ($y = 0.2 - 0.6$) synthesized by the Pechini method, according to XRD, are well-crystallized solid solutions having ortho-rhombic symmetry with s.g. Pnma (see Fig. 1a). The volume of the unit cell of complex oxides varied from 224 to 227 Å^3 (see Table 1). With an increase in the degree of cobalt substitution, the volume of the unit cell showed a slight decrease, which can be explained by lower values of the radii of Co^{3+} cations (0.59 ± 0.05 Å for Co^{3+} and 0.62 ± 0.02 Å for Mn^{3+}), the number of which presumably increases with a growth in the pro-portion of cobalt in the solid solution. The electroneutrality in the structure is mainly provided by the formation of oxygen vacancies and Mn4+ cations, which has already been shown for $La_{1-x}Ca_xMnO_{3\pm\delta}$ [28], although the formation of Co^{2+} cations is also allowed, as in $LaMn_{1-y}Co_yO_{3\pm\delta}$ [29].

TABLE 1. Unit cell parameters of $La_{0.6}Ca_{0.4}Mn_{1-y}Co_yO_{3\pm\delta}$ in initial state

Sample	V, Å^3	D, Å	ε	S, m^2/g
$La_{0.6}Ca_{0.4}Mn_{0.8}Co_{0.2}O_3$	227.37	590	0.0017	7.7
$La_{0.6}Ca_{0.4}Mn_{0.7}Co_{0.3}O_3$	226.64	437	0.001	9.5
$La_{0.6}Ca_{0.4}Mn_{0.6}Co_{0.4}O_3$	225.69	470	0.003	11.5
$La_{0.6}Ca_{0.4}Mn_{0.5}Co_{0.5}O_3$	224.71	380	0.0035	11.8
$La_{0.6}Ca_{0.4}Mn_{0.4}Co_{0.6}O_3$	224.33	433	0.0026	13.7

According to XRD data, the particles of solid solutions consist of crystallites with sizes of 20 – 30 nm (see Table 1), correlating with the particle size, according to the HRTEM data, the average particle size is 40 – 50 nm (Fig. 1b). Based on calculations, the micro-distortion parameter increases slightly in samples with a high content of Co cations. The specific surface area increases with the cobalt content and correlates with a decrease in the size of crystallites and particles, respectively (Table 1). The performed mapping of chemical elements did not show significant deviations from the chemical composition (Fig. 1c). A more detailed study by the HRTEM method showed that the samples of this series are well crystallized and have a perovskite structure in orthorhombic modification (Fig. 1d).

In situ XRD experiments in hydrogen containing atmosphere have shown that partial decomposition is characteristic for perovskite-like oxides of these compositions, and the effect of a reducing medium leads to a decomposition mechanism different from that observed in an only He medium [26]. $La_{0.6}Ca_{0.4}Mn_{1-x}Co_xO_3$ samples similarly to

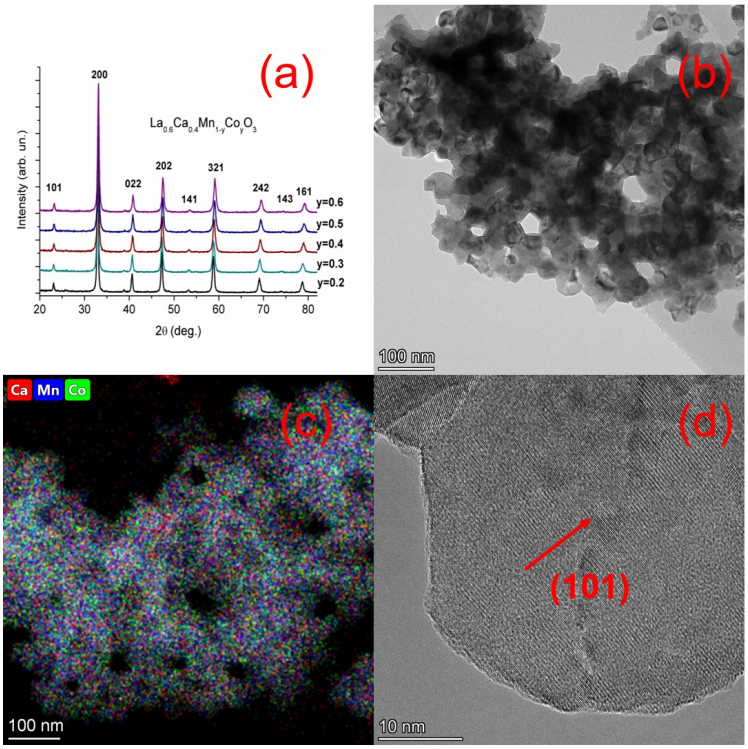

FIG. 1. XRD patterns of $La_{0.6}Ca_{0.4}Mn_{1-y}Co_yO_{3\pm\delta}$ in initial state (a). HRTEM images of sample morphology (b) and microstructure (c), EDX mapping for $La_{0.6}Ca_{0.4}Mn_{0.5}Co_{0.5}O_3$ sample (d)

$La_{0.5}Ca_{0.5}Mn_{0.5}Co_{0.5}O_3$ release lattice oxygen when heated to 600 °C in a helium environment, which leads to a visible increase in the cell parameters. Further heating to 750 °C leads to the decomposition of the complex oxide with the formation of CaO and CoO particles on the surface of the perovskite (Fig. 2a). At the same time, the structure of the perovskite type is quite stable with minor changes in chemical composition. The size of the crystallites also does not change significantly and remains around the same values (about 55 nm for $La_{0.6}Ca_{0.4}Mn_{0.8}Co_{0.2}O_3$).

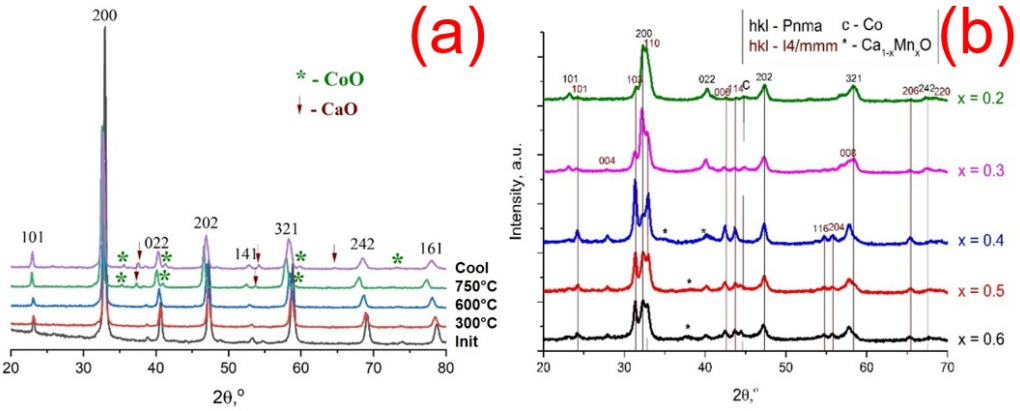

FIG. 2. In situ XRD patterns of $La_{0.6}Ca_{0.4}Mn_{0.8}Co_{0.2}O_3$ in He atmosphere (a), XRD patterns of $La_{0.6}Ca_{0.4}Mn_{1-y}Co_yO_3$ after treatments in hydrogen containing atmosphere (b)

At the same time, strong asymmetric broadenings of the perovskite phase reflexes are observed in the hydrogen medium (Fig. 2b), further splitting of which occurs at 550 – 600 °C. The phase composition of the system most likely includes perovskite-like solid solutions of orthorhombic symmetry, with different chemical compositions and, as a result, unit cell parameters. The differences in composition are primarily due to different oxygen content, while the formation of cobalt nanoparticles on the surface (S.g. Fm3m, PDF No. 15-806), as well as Ca_2MnO_4 (PDF No. 78-1031) and CaO (PDF No. 37-1497) shows that changes occur in the cationic sublattices. At 600 °C, the transformation of part of the initial solid solution into the phase of ordered perovskite (Raddlesden–Popper) of tetragonal symmetry (structural type La_2CoO_4, s.g. I4/mmm, PDF No. 34-1081) is also observed.

For the sample with the highest content of Mn cations – $La_{0.6}Ca_{0.4}Mn_{0.8}Co_{0.2}O_3$, a similar transformation is also observed, although it is expressed to a lesser extent (Fig. 2a). With a decrease in the proportion of manganese cations in the structure to 0.6 – 0.4, the intensity of the peaks of the ordered perovskite phase increases significantly and it becomes larger, which makes it possible to make conclusion about the key role of cobalt in this transformation. An increase in the cobalt content in the solid solution also reduces the temperature at which structural transformations begin: for example, in the case of $La_{0.6}Ca_{0.4}Mn_{0.4}Co_{0.6}O_3$ decomposition begins at 450 °C (Fig. 3a), while for $La_{0.6}Ca_{0.4}Mn_{0.6}Co_{0.4}O_3$ the process does not begin earlier than 550 °C (see Fig. 3b) for $La_{0.6}Ca_{0.4}Mn_{0.5}Co_{0.5}O_3$ it begins at 500 °C and for $La_{0.6}Ca_{0.4}Mn_{0.8}Co_{0.2}O_3$ – 600 °C.

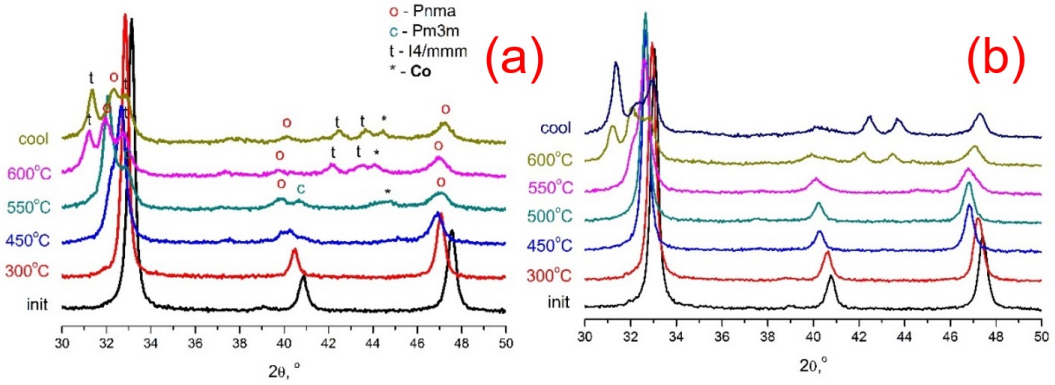

FIG. 3. In situ XRD patterns obtained in hydrogen containing atmosphere $La_{0.6}Ca_{0.4}Mn_{0.4}Co_{0.6}O_3$ (a) and $La_{0.6}Ca_{0.4}Mn_{0.6}Co_{0.4}O_3$ (b)

Table 2 shows the parameters of the unit cell (in the form of reduced volumes, for clarity) before and after heat treatment in a reducing medium. The parameters for one of the phases after reducing are closer to the initial values, which allows us to assert the heterogeneous layered nature of reducing medium. For the forming phase of an ordered perovskite, the cell parameter is slightly less than that for La_2CoO_4. Apparently, this is due to the formation of a solid solution, with the assumed composition of $La_{2-x}Ca_xCoO_{4-\delta}$. The difference of 1 Å^3 allows us to assert that the proportion of calcium in it is relatively small, however, the presence of manganese cations in it is not excluded, which increase the volume of the cell, and therefore it is difficult to judge the exact ratio of calcium in the structure. For the second phase based on perovskite, the parameters are close to those for $La_{0.85}Ca_{0.15}MnO_3$.

TABLE 2. The reduced volume of the unit cell of the initial and reduced samples

Sample	$V/Z_{\text{init.}}$, Å^3	$V/Z_{\text{tetr.}}$, Å^3	$V/Z_{\text{ort.}}$, Å^3
$La_{0.6}Ca_{0.4}Mn_{0.8}Co_{0.2}O_3$	56.84	94.42	58.04
$La_{0.6}Ca_{0.4}Mn_{0.7}Co_{0.3}O_3$	56.66	94.39	58.12
$La_{0.6}Ca_{0.4}Mn_{0.6}Co_{0.4}O_3$	56.34	94.36	59.33
$La_{0.6}Ca_{0.4}Mn_{0.5}Co_{0.5}O_3$	56.12	94.26	59.40
$La_{0.6}Ca_{0.4}Mn_{0.4}Co_{0.6}O_3$	55.93	94.50	59.79

Apparently, the observed change in the structure of perovskite occurs due to the reduction of cobalt and manganese cations, in particular, one of the key transformations here is $Co^{3+} \rightarrow Co^{2+}$. On the surface, under the influence of the medium, these cations are further reduced to a metallic state and migrate to the surface, forming surface defects and thereby promoting the process of H_2 diffusion and reduction of the complex oxide. Taking into account the XRD data and the possible heterogeneity of perovskite recovery, the phase of ordered perovskite based on La_2CoO_4 is located mainly in the near-surface layers of particles, since it is characterized by a high content of Co^{2+} in its composition, while the phase of disordered perovskite is located closer to the center of the particles.

At the same time, this process demonstrates partial reversibility in the case of repeated heat treatment in an oxygen-containing atmosphere, as previously shown [27]. A similar behaviour was shown by the $La_{0.6}Ca_{0.4}Mn_{1-y}Co_yO_3$ systems: for the phases, a decrease in cell parameters and an overlap of reflexes were observed, and only the perovskite phase with orthorhombic symmetry was observed relatively reliably in the phase composition, the volume of the cell of which was 2 – 3 Å^3 larger than the volume of the initial phase (see Table 2). The process of restoring the structure is mainly associated with the return of oxygen to the structure of the complex oxide, which is reflected in the thermogravimetry

curves (Fig. 4a). This process is also clearly visible on the diffractograms of the initial sample $La_{0.6}Ca_{0.4}Mn_{0.4}Co_{0.6}O_3$ in comparison with reduced in hydrogen and reoxidized in air (Fig. 4b). Thermogravimetric curves recorded for the corresponding states in the air atmosphere. For the initial sample of the reduced form, the presence of an oxygen release peak at 600 °C was noted. This process, as it was shown earlier [27], leads to destabilization of the structure of complex oxides. For the recovered sample, there is also an intense peak of oxygen absorption in the region of 300 °C, which is formed due to at least the contribution of two processes: oxidation of complex oxides with a perovskite structure and oxidation of cobalt metal nanoparticles to Co_3O_4.

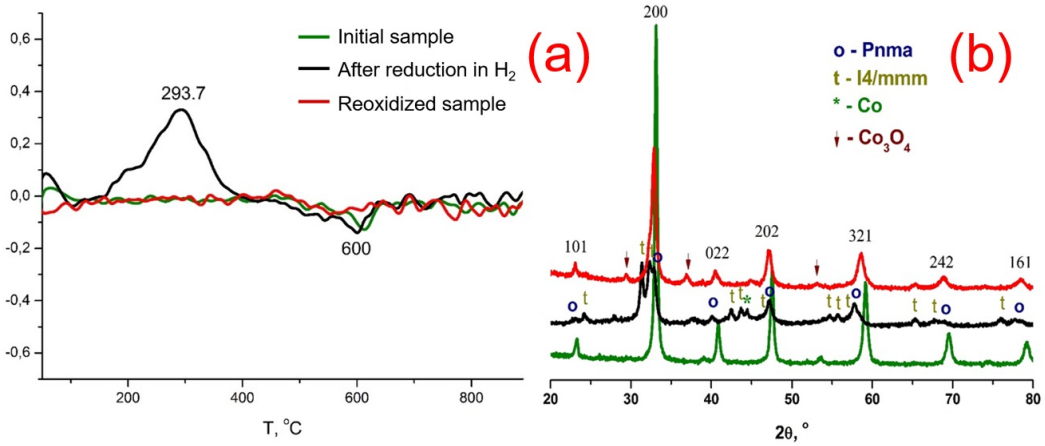

FIG. 4. TG curves for the initial, reduced and oxidized $La_{0.6}Ca_{0.4}Mn_{0.5}Co_{0.5}O_3$ in the air atmosphere (a) and comparative XRD patterns of $La_{0.6}Ca_{0.4}Mn_{0.4}Co_{0.6}O_3$, the green curve corresponds to the original sample, the black curve corresponds to the reduced one in hydrogen, the red curve corresponds to the reoxidized sample in the air stream (b)

In situ XRD studies show that upon reaching a temperature of 300 °C in air oxygen (Fig. 5b), the intensity of the tetragonal phase reflex 100 changes due to the contribution of the orthorhombic reflex 200 to the signal, and some of the other reflexes related to the orthorhombic phase shift towards large angles, which indicates a decrease in the cell parameter of this phase. With a further increase to 600 °C, the reflexes of the ordered perovskite disappear, while at a lower temperature (for example, 450 °C) this process is not carried out. This suggests that the mechanism of "reoxidation" of $La_{0.6}Ca_{0.4}Mn_{1-x}Co_xO_3$ proceeds in at least two stages: through oxygen saturation and "oxidation" of the structure of nonstoichiometric orthorhombic perovskite at 300 °C, and then through subsequent restructuring of the layer of ordered perovskite. Most likely, the transition to an unordered state requires a higher temperature, while the phase of an ordered perovskite can be saturated with oxygen to certain limits while maintaining this state, and also serve as an effective oxygen conductor for deeper layers, as a result of which their saturation and change occur. The La_2CoO_4-based phase may also hinder further reduction of perovskite, as it may impede the diffusion of cobalt cations to the surface, due to which the reduction in hydrogen proceeds inhomogeneously.

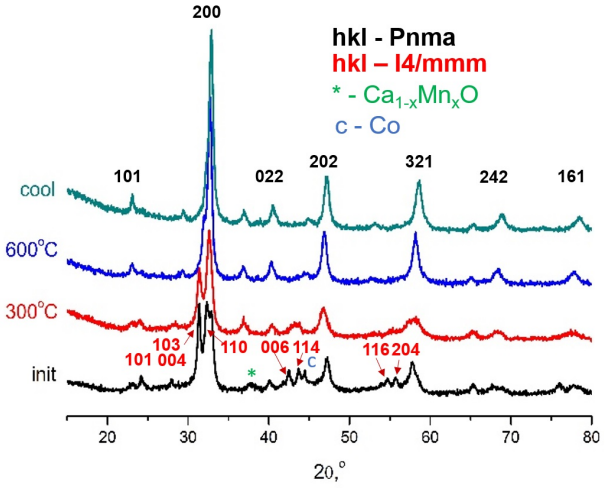

FIG. 5. In situ XRD patterns demonstrating the processes of reoxidation of solid solutions $La_{0.6}Ca_{0.4}Mn_{0.6}Co_{0.4}O_3$

Significant changes in the microstructure are clearly visible on EDX mapping (Fig. 6a). In the sample, after treatment in a reducing atmosphere, the release of cobalt particles on the surface of the perovskite phase is observed. These particles have approximately the same size on the order of 10 nm and a uniform distribution over the surface of the perovskite. Also, according to the EDX mapping data, it can be seen that there are zones of enrichment with calcium cations, which corresponds to the XRD data on the coexistence of two phases with different chemical compositions. The morphology of the sample after reoxidation to 600 °C changes significantly, the particles of both the perovskite phase and cobalt oxide particles are enlarged (Fig. 6b). At the same time, Ca cation enrichment zones are observed, which indicates that Ca does not fully return to the perovskite structure. It is worth noting that according to HRTEM data, calcium oxide forms a film coating (Fig. 6c) and therefore the signal from this phase is practically not observed on diffractograms. In general, the structure of perovskite undergoes significant changes, expressed in the presence of a large number of micro-distortions and a decrease in the degree of crystallinity (Fig. 6d).

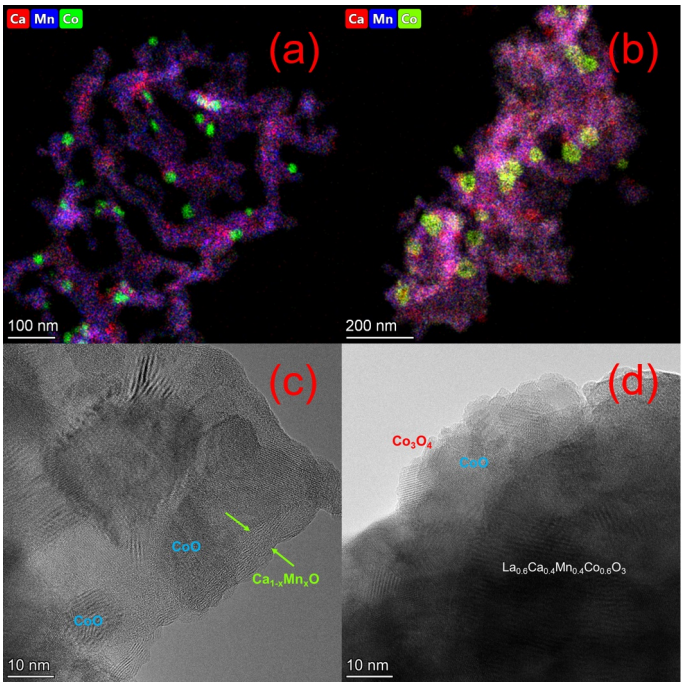

FIG. 6. EDX mappings and HRTEM images of $La_{0.6}Ca_{0.4}Mn_{0.4}Co_{0.6}O_3$ sample after treatments in hydrogen containing medium (a,c) and after subsequent oxidation at a temperature of 600 °C (b, d)

4. Conclusion

The effect of the reducing medium on the structure of complex oxides $La_{0.6}Ca_{0.4}Mn_{1-x}Co_xO_3$ was studied by in situ XRD and HRTEM methods. It is shown that the influence of the reducing medium at temperatures of 450 – 600 °C leads to the formation of ordered phases based on the Radlesdenne–Popper structure, while the content of this phase strongly depends on the initial composition of perovskite. In addition, the high content of Mn cations in the perovskite sublattice increases the temperature of such transitions.

The effect of oxygen treatment of the reduced samples at temperatures of 300 – 600 °C leads to a partial return of the multicomponent system to its original state. Thermogravimetry has shown that oxygen is absorbed by these systems in the temperature range 200 – 350 °C, which leads to a partial return to the perovskite structure. The study of the microstructure by the HRTEM method showed that during the treatment of solid solutions in hydrogen, cobalt particles and a $Ca_{1-x}Mn_xO$ layers coating are formed on the surface of the perovskite phase. After calcination in air, particles of the Co and Ca-containing phase remain on the surface of the perovskite phase, which also indicates an incomplete return of the structure of solid solutions to its initial state.

References

[1] Xia W., Pei Z., Leng K., Zhu X. Research Progress in Rare Earth-Doped Perovskite Manganite Oxide Nanostructures. *Nanoscale Research Letters*, 2020, **15** (1), 9.

[2] Zhu J., Li H., Zhong L., Xiao P., Xu X., Yang X., Zhao Z., Li J. Perovskite Oxides: Preparation, Characterizations, and Applications in Heterogeneous Catalysis. *ACS Catalysis*, 2014, **4** (9), P. 2917–2940.

[3] Grabowska E. Selected perovskite oxides: Characterization, preparation and photocatalytic properties-A review. *Applied Catalysis B: Environmental*, 2016, **186**, P. 97–126.

[4] Bashan V., Ust Y. Perovskite catalysts for methane combustion: applications, design, effects for reactivity and partial oxidation. *Int. J. of Energy Research*, 2019, **43** (14), P. 7755–7789.
[5] Najjar H., Batis H. Development of Mn-based perovskite materials: Chemical structure and applications. *Catalysis Reviews*, 2016, **58** (3), P. 371–438.
[6] Keav S., Matam S., Ferri D., Weidenkaff A., Keav S., Matam S.K., Ferri D., Weidenkaff A. Structured Perovskite-Based Catalysts and Their Application as Three-Way Catalytic Converters—A Review. *Catalysts*, 2014, **4** (3), P. 226–255.
[7] Khaledian H.R., Zolfaghari P., Nezhad P.D.K., Niaei A., Khorram S., Salari D. Surface modification of $LaMnO_3$ perovskite supported on CeO_2 using argon plasma for high-performance reduction of NO. *J. of Environmental Chemical Engineering*, 2021, **9** (1), 104581.
[8] Shen Q., Dong S., Li S., Yang G., Pan X. A Review on the Catalytic Decomposition of NO by Perovskite-Type Oxides. *Catalysts*, 2021, **11** (5), 622.
[9] Wu Y., Liu H., Li G., Jin L., Li X., Ou X., Dong L., Jin G., Li B. Tuning composition on B sites of $LaM_{0.5}Mn_{0.5}O_3$ (M = Cu, Co, Fe, Ni, Cr) perovskite catalysts in NOx efficient reduction. *Applied Surface Science*, 2020, **508**, 145158.
[10] Afify M.S., Faham M.M.E., Eldemerdash U., El-Dek S.I., Rouby W.M.A.E. Effects of Ag doping on $LaMnO_3$ photocatalysts for photoelectrochemical water splitting. *Applied Physics A: Materials Science and Processing*, 2022, **128** (10), P. 1–12.
[11] Jawhari A.H., Hasan N., Radini I.A., Narasimharao K., Malik M.A. Noble Metals Deposited $LaMnO_3$ Nanocomposites for Photocatalytic H_2 Production. *Nanomaterials*, 2022, **12** (17), 2985.
[12] Kida T., Guan G., Yoshida A. $LaMnO_3$/CdS nanocomposite: a new photocatalyst for hydrogen production from water under visible light irradiation. *Chemical Physics Letters*, 2003, **371** (5–6), P. 563–567.
[13] Garba Z.N., Zhou W., Zhang M., Yuan Z. A review on the preparation, characterization and potential application of perovskites as adsorbents for wastewater treatment. *Chemosphere*, 2020, **244**, 125474.
[14] Yiğiter İ.E., Pişkin B. Investigation into Ca-Doped $LaMnCoO_3$ Perovskite Oxides for Thermochemical Water Splitting. *JOM*, 2022, **74** (12), P. 4682–4694.
[15] Kwon O., Kim Y.I., Kim K., Kim J.C., Lee J.H., Park S.S., Han J.W., Kim Y.-M., Kim G., Jeong H.Y. Probing One-Dimensional Oxygen Vacancy Channels Driven by Cation–Anion Double Ordering in Perovskites. *Nano Letters*, 2020, **20** (11), P. 8353–8359.
[16] Gan L.-Y., Akande S.O., Schwingenschlögl U. Anisotropic O vacancy formation and diffusion in $LaMnO_3$. *J. Mater. Chem. A*, 2014, **2** (46),
[17] Zheng J., Zhao H., Guo X., Jin X., Wang L., Dong S., Chen J. Enhanced Electrochemical Performance of $LaMnO_3$ Nanoparticles by Ca/Sr Doping. *Coatings*, 2023, **14**, 20.
[18] Yin X., Zhang R., Zhang Y., Wang S., Shen L. Enhanced reactivity of methane partial oxidation of nickel doped $LaMnO_{3+\delta}$ perovskites for chemical looping process. *Int. J. of Hydrogen Energy*, 2024, **71**, P. 481–492.
[19] Politov B.V., Shalamova A.M., Shein I.R., Suntsov A.Y. Exploring oxygen non-stoichiometry in presumably stoichiometric double perovskites: the case study for $LaCu_{0.5}Mn_{0.5}O_{3-\delta}$. *Acta Materialia*, 2023, **250**, 118872.
[20] Vieten J., Bulfin B., Huck P., Horton M., Guban D., Zhu L., Lu Y., Persson K.A., Roeb M., Sattler C. Materials design of perovskite solid solutions for thermochemical applications. *Energy & Environmental Science*, 2019, **12** (4), P. 1369–1384.
[21] Liu X., Wang S., Liao Y., Lei M., Fang X., Xu X., Wang X. La/Mn molar ratio tuning the activity of La–Mn perovskites for CO and propane oxidation. *J. of the Energy Institute*, 2024, **114**, 101595.
[22] Zhao A., Ren Y., Wang H., Qu Z. Enhancement of toluene oxidation performance over La1-CoO3- perovskite by lanthanum non-stoichiometry. *J. of Environmental Sciences*, 2023, **127**, P. 811–823.
[23] Jiang Y., Li Z., Zhu T., Li D., Wang H., Zhu X. Oxygen Storage Characteristics and Redox Behaviors of Lanthanum Perovskite Oxides with Transition Metals in the B-Sites. *Energy & Fuels*, 2023, **37** (13), P. 9419–9433.
[24] Mantzavinos D. Oxygen stoichiometries in $La_{1-x}Sr_xCo_{1-y}Fe_yO_{3-\delta}$ perovskites at reduced oxygen partial pressures. *Solid State Ionics*, 2000, **134** (1–2), P. 103–109.
[25] Nadeev A.N., Tsybulya S.V., Gerasimov E.Y., Isupova L.A. High-temperature phase transitions in the $La_{0.25}Sr_{0.75}FeO_{3-\delta}$ solid solution with a perovskite structure. *J. of Structural Chemistry*, 2009, **50**, P. 108–113.
[26] Gerasimov E.Yu., Rogov V.A., Prosvirin I.P., Isupova L.A., Tsybulya S.V. Microstructural Changes in $La_{0.5}Ca_{0.5}Mn_{0.5}Fe_{0.5}O_3$ Solid Solutions under the Influence of Catalytic Reaction of Methane Combustion. *Catalysts*, 2019, **9**, 563.
[27] Kapishnikov A.M., Bespalko Yu.N., Shuvarakova E.I., Tsybulya S.M., Isupova L.A., Gerasimov E.Yu. Influence of Oxygen Nonstoichiometry on the Structural Stability of $La_{1-x}Ca_xMn_{0.5}Co_{0.5}O_3$ Complex Oxides ($x = 0.2 - 0.6$) Subjected to Heat Treatment in He. *J. of Structural Chemistry*, 2024, **65**, P. 107–116.
[28] Isupova L.A., Gerasimov E.Yu., Zaikovskii V.I., Tsybulya S.V. Effect of the reaction medium on the structure of the $La_{1-x}Ca_xMnO_3$ ($x = 0 - 1$) solid solutions prepared by the pechini method. *Kinetics and Catalysis*, 2011, **52**, P. 104–110.
[29] Flores-Lasluisa J.X., Huerta F., Cazorla-Amorys D., Morallyn E. Structural and morphological alterations induced by cobalt substitution in $LaMnO_3$ perovskites. *J. of Colloid and Interface Science*, 2019, **556**, P. 658–666.

Submitted 19 November 2024; accepted 12 December 2024

Information about the authors:

Alexander V. Kapishnikov – Boreskov Institute of Catalysis SB RAS, Lavrentieva Ave, 5, Novosibirsk, 630090, Russia; ORCID 0000-0002-3921-5629; avl97@mail.ru

Evgeny Yu. Gerasimov – Boreskov Institute of Catalysis SB RAS, Lavrentieva Ave, 5, Novosibirsk, 630090, Russia; ORCID 0000-0002-3230-3335; gerasimov@catalysis.ru

Conflict of interest: the authors declare no conflict of interest.